INT. J. NUM. METH. HEAT FLUID FLOW, VOL. 2, 215–226 (1992)

SOLUTIONS OF SOME AXISYMMETRIC LOW STEFAN NUMBER MELTING PROBLEMS BY AN IMPROVED FINITE DIFFERENCES METHOD

M. SOKOLOV AND Y. KEIZMAN

Department of Fluid Mechanics and Heat Transfer, Faculty of Engineering and Gordon Center for Energy Studies, Tel Aviv University, Ramat Aviv 69978, Israel

ABSTRACT

The use of explicit finite difference schemes for low Stefan number problems with moving interface was largely abandoned because they require small time intervals (large CPU time) to obtain accurate non-oscillatory solutions. This paper uses these type of schemes for better estimations of the dynamics of the solid–liquid interface. The scheme in which time and radial intervals are constant, uses a local, continuous, time-dependent radial coordinate to define the instantaneous location of the interface. Taylor series expansions which result in a polynomial fit are used for forward and backward interpolation of temperatures of nodal points in the vicinity of the interface. A distinction is made between the left and right position of the interface relative to the closest nodal point. The algorithm handles accurately and effectively the non-linearities near the interface thus producing accurate stable solutions with relatively low CPU time. The scheme which obviously may be applied to large Stefan number problems, is also suitable for time dependent boundary conditions as well as temperature dependent physical properties. The results obtained by the scheme were in excellent agreement with ones derived from an approximate analytical solution which is applicable in the low Stefan number range.

KEY WORDS Melting Stefan problems

INTRODUCTION

Unsteady Stefan problems of heat conduction accompanied by fusion or solidification are of interest in a large number of engineering applications such as metal or plastics casting, freezing of biological material or foodstuffs and latent heat thermal storage systems. Accordingly, there is a wealth of technical information in the literature on this subject which include various models, analyses, simulations and methods of solution[7]. The main cause of complexity in such problems is associated with the non-linear nature of the liquid–solid interface motion.

During the 1960s, the explicit finite differences method was used to solve problems of simple geometries and boundary conditions. However, with the need to tackle problems of higher degree of complexity, the scheme which requires a large CPU, was almost abandoned in favour of other methods. Since then, CPU prices have fallen sharply such that this handicap is no longer a serious one. Thus the advantages the explicit scheme should be reconsidered.

One of the explicit finite difference scheme tracks a local, time dependent moving boundary between neighbouring nodes on a fixed space grid. Crank[1] suggested Lagrangian interpolation for near interface approximation in explicit method and used the scheme for solutions of one-dimensional problems.

Murray and Landis[2] tackled the problem of one dimensional metal slab solidifcation with large (>1) Stefan number. In one of their schemes they used a moving-grid method with a

0961–5539/92/030215–12$2.00

Received May 1991
Revised October 1991

variable time step and in the other, fixed grid and constant time intervals were used. The latter method in which linear interpolation between the nodes was used, resulted in a solution which led Yao and Prusa[4] to conclude that 'despite Murray and Landis's success the ad hoc boundary conditions at the solid–liquid interface generally do not completely neutralize pathological behavior in the predicted solution from fixed-grid methods'. Springer and Olson[3] later extended this technique to a cylindrical geometry where backward and forward second order Lagrangian interpolation were used to prevent singularities near the interface. Their Lagrangian interpolation[3] which disregards the region between the interface and its closest nodal point, is capable of handling large Stefan (flux) number problems where such neglect is justified. For low Stefan number problems the form of interpolation suggested by Springer and Olson[3] results in oscillation of the temperature field solution.

The solutions presented here for phase transition in cylindrical geometry with a low Stefan numbers, involves a refinement of the Springer and Olson[3] treatment at the vicinity of the interface. The modified finite difference scheme is capable of solving a wide class of initial and boundary conditions problems with a relatively simple algorithm. It results in a non-oscillatory stable solution. Taylor series expansion of temperatures near the interface takes into account the location of the interface either to the left or to the right of the nearest nodal point. Thus an accurate coupling conditions between the solid and liquid regions are provided and temperature distributions are continuously updated while the interface propagates.

For simplicity sake, thermal conductivities k_l and k_s, heat capacities c_l and c_s of the liquid and solid phases respectively, are assumed to be constant. With only a slight obvious modification in the numerical solution scheme, these properties may be allowed to become temperature dependent. Thermal stresses effects are assumed negligible since densities ρ_l and ρ_s are assumed equal and temperature independent. Convection effects within the liquid phase are neglected and the heat conduction is assumed to be one dimensional.

STATEMENT OF THE PROBLEM AND GOVERNING EQUATIONS

A phase changing material (PCM) confined between two concentric cylinders (*Figure 1*) is initially at an arbitrary axisymmetric temperature distribution (usually below the melting temperature). The external surface which is exposed to the ambient temperature, is subjected to an axisymmetric heat flux which eventually causes a symmetric melting (or solidification) process. The heat fluxes and ambient temperatures boundary conditions may be time dependent. Usually heat supply will be assumed at the outer surface and heat removal from the inner. Thus, starting at the outer circumference, a melted zone develops in regions where temperatures have

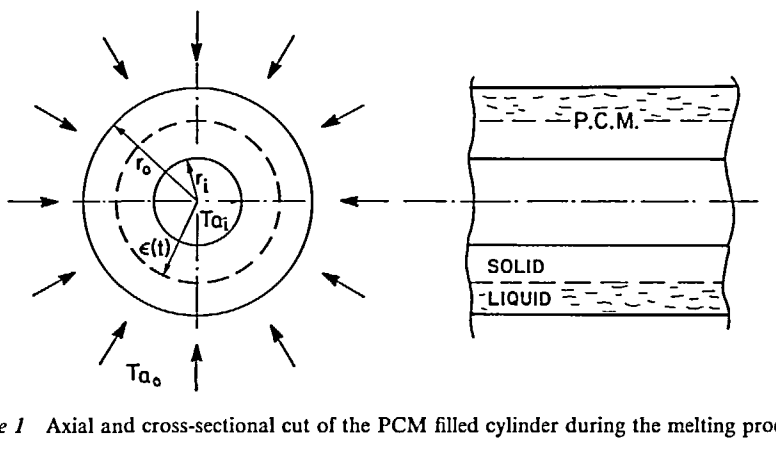

Figure 1 Axial and cross-sectional cut of the PCM filled cylinder during the melting process

risen above the melting point. With the continued heat transfer into the system, the interface between the liquid and solid region moves inward while a temperature gradient near the interface establishes the conditions for its motion.

The above description may be summed up by the following characteristics of the problem: (1) the geometry and boundary conditions are axisymmetric; (2) the phase transition occurs at single temperature; (3) heat transfer—by conduction in the material; (4) the density of the solid and liquid are the same $\rho=\rho_l=\rho_s$.

With temperature $T(r,t)$ being the only dependent variable, Fourier's heat conduction[5,6] equations for each of the regions may be written provided the interface radial position $\varepsilon(t)$ (see *Figure 1*) is known. Thus for the inner solid region:

$$\frac{1}{\alpha_s}\frac{\partial T_s}{\partial t}=\frac{\partial^2 T_s}{\partial r^2}+\frac{1}{r}\cdot\frac{\partial T_s}{\partial r} \qquad \text{for} \quad r_i<r<\varepsilon(t) \tag{1}$$

Similarly, for the outer liquid region:

$$\frac{1}{\alpha_l}\frac{\partial T_l}{\partial t}=\frac{\partial^2 T_l}{\partial r^2}+\frac{1}{r}\cdot\frac{\partial T_l}{\partial r} \qquad \text{for} \quad r_0>r>\varepsilon(t) \tag{2}$$

At all times, the interface is at the melting temperature, thus:

$$T_s(\varepsilon(t),t)=T_l(\varepsilon(t),t)=T_f \tag{3}$$

The radial speed of propagation of the interface is determined[5] by an energy balance across the interface which is given by:

$$\frac{\mathrm{d}\varepsilon(t)}{\mathrm{d}t}=\frac{1}{\rho L}\left[k_s\frac{\partial T_s}{\partial r}\bigg|_{\varepsilon(t)}-k_l\frac{\partial T_l}{\partial r}\bigg|_{\varepsilon(t)}\right] \tag{4}$$

$T(r,t)$ which is the solution for the stated problem is superimposed by the temperature distribution in the two phases such that:

$$T(r,t)=\begin{cases}T_l(r,t) & \text{for } \varepsilon(t)<r<r_0\\ T_s(r,t) & \text{for } r_i<r<\varepsilon(t)\end{cases} \tag{5}$$

This solution must satisfy the heat conduction equations (1) and (2) as well as the interface relations (3) and (4) provided proper boundary conditions at the inner and outer radii as well as initial conditions $T(r,0)$ have been satisfied. These boundary and initial conditions are generally written in the form:

$$k_s, l\frac{\partial T}{\partial r}\bigg|_{r_i}, o=h_i, o[T_{a_i}, o-T(r_i,o,t)]+F_i,o(t) \tag{6}$$

$$T(r,0)=G(r) \tag{7}$$

where F is heat flux on the surface, and the indices i, o are for the inner or outer radii ($k_i\equiv k_s$, $k_o\equiv k_l$), respectively. When either of the surfaces is thermally insulated the corresponding left hand side of (6) vanishes.

DIMENSIONLESS REPRESENTATION

In order to maintain generality of the problem, the following dimensionless variables are defined:

$$\theta=\frac{T-T_f}{T_f-T_i}; \qquad \bar{r}=\frac{r-r_i}{r_i}; \qquad \bar{\varepsilon}=\frac{\varepsilon-r_i}{r_i}; \qquad \bar{t}=\frac{(T_f-T_i)}{\rho L r_i^2}k_s t \tag{8}$$

$$St_{si}=\frac{C_{ps}(T_f-T_i)}{L}; \qquad St_{li}=\frac{C_{pl}(T_f-T_i)}{L}; \qquad K=\frac{k_l}{k_s} \tag{9}$$

Substituting these variables into (1), (2), (3) and (4) the basic equation for $\theta(\bar{r},\bar{t})$ assumes a dimensionless form:

$$St_{si}\frac{\partial\theta_s}{\partial\bar{t}}=\frac{\partial^2\theta_s}{\partial\bar{r}^2}+\frac{1}{1+\bar{r}}\cdot\frac{\partial\theta_s}{\partial\bar{r}} \qquad 0<\bar{r}<\bar{\varepsilon}(\bar{t}) \tag{10}$$

$$\frac{St_{li}}{K}\frac{\partial\theta_l}{\partial\bar{t}}=\frac{\partial^2\theta_l}{\partial\bar{r}^2}+\frac{1}{1+\bar{r}}\cdot\frac{\partial\theta_l}{\partial\bar{r}} \qquad \bar{\varepsilon}(\bar{t})<\bar{r}<\bar{r}_0 \tag{11}$$

$$\theta_l=\theta_s=0 \qquad \text{at} \quad \bar{r}=\bar{\varepsilon}(\bar{t}) \tag{12}$$

$$\frac{d\bar{\varepsilon}}{d\bar{t}}=\left(\frac{\partial\theta_s}{\partial\bar{r}}-K\frac{\partial\theta_l}{\partial\bar{r}}\right)_{\bar{\varepsilon}} \tag{13}$$

respectively. The boundary condition in (6) will assume the form:

$$\left.\frac{\partial\theta}{\partial\bar{r}}\right|_{\bar{r}_i,o}=Bi_i,o(\theta_{a_i},o-\theta(\bar{r}_i,o,\bar{t}))+\bar{F}_i,o \tag{14}$$

where $Bi_i,o=(h_i,or_i)/k_s,l$ and $\bar{F}_i,o=(F_i,o(t)\cdot r_i/((T_f-T_i)\cdot k_s,l)$. The initial condition (7) will be transformed into:

$$\theta(\bar{r},0)=G(\bar{r}) \tag{15}$$

MODIFICATION OF THE SPRINGER AND OLSON[3] SCHEME

The Springer and Olson[3] scheme does not distinguish between $\zeta>0$ or $\zeta<0$ (see *Figure 2* for notations) in evaluating the temperature derivatives and therefore the speed of the interface $\varepsilon(t)$.

The modification in this work which consists of differentiation between the two situations, enables a more precise evaluation of the time and space derivatives near the interface. Such refinement allows larger time intervals while maintaining the stability of the solution. Details of the modified scheme can be found in Keizman's work[8].

The modified finite difference method for the moving boundary problem was incorporated in a numerical scheme. The program can handle a large variety of axisymmetric problems which includes low or large Stefan numbers, time dependent boundary condition and temperature dependent physical properties of the PCM. The program consists of three major parts. In the first, heat-conduction equations are solved to determine temperature profiles in either of the two phases (or in one if melting temperature has not yet been reached). The second part uses the profiles obtained in the first part to evaluate the interface speed of propagation. The third updated the conditions under which the cycle advances as time progresses. Thus, prior to the

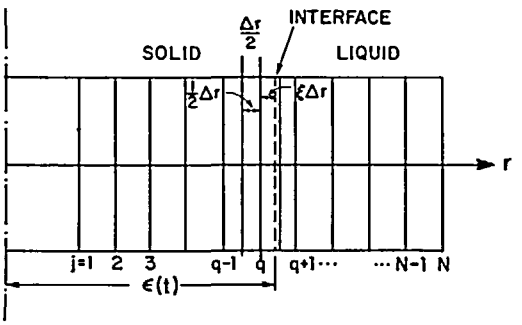

Figure 2 Grid configuration during the melting process

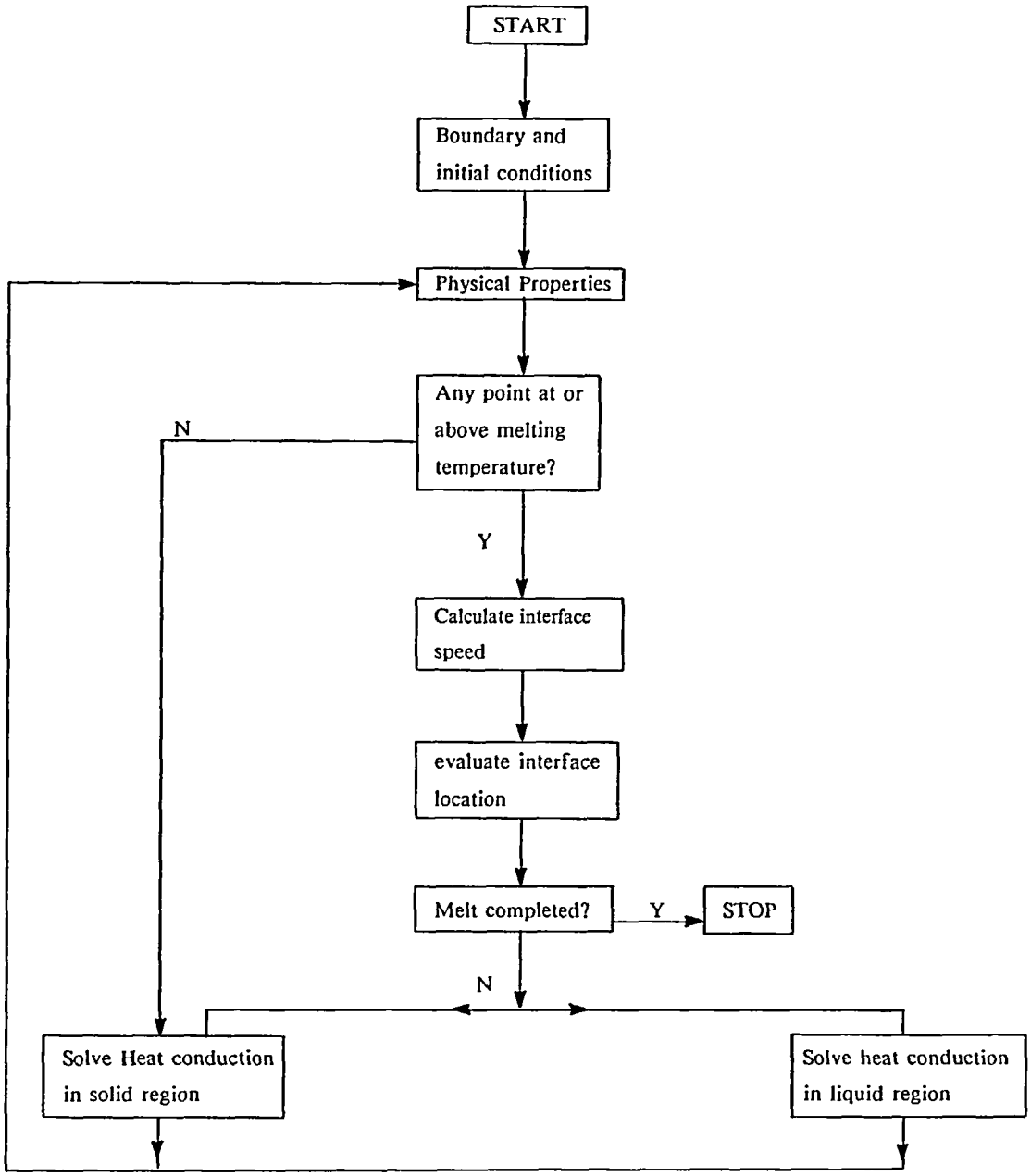

Figure 3 Flow chart for the numerical scheme

onset of melting, the procedure proceeds by updating the temperature distribution. Once phase change has been detected, the temperature profiles are updated by using current interface position as a boundary condition for the heat conduction equations. Each of the regions is then solved with proper updated physical properties. The essentials of the program are shown in the block diagram depicted in *Figure 3*.

MESH SIZE AND ERROR ANALYSIS

One of the major advantages of the modified scheme, is that it may be used with relatively large radial increments. The interface position which is defined *within* the radial intervals by the continuous variable $\zeta(t)$ (*Figure 2*), provides a higher degree of accuracy in the determination of the discontinuity in the temperature gradients. However, it is still expected that the mesh size in the radial coordinate will effect the accuracy of the obtained results. Through the numerical stability requirement, the determination of the radial mesh size has also a direct bearing on the time intervals, such that a finer radial grid means also a finer time interval. In order to determine the effect of the radial mesh size on the results, two test cases were run. The first consists of a cylinder insulated on both radii, initially in a solid phase at the melting temperature and with dimensions and physical parameters corresponding to case A in *Tables 1* and *2*. A constant heat flux F_o causes the PCM to melt within the time t_{ins_m} required by the flux to provide the latent heat. This time is given by:

$$t_{\text{ins}_m}=\rho L\pi(r_o^2-r_i^2)/2\pi r_o F_o \tag{16}$$

or:

$$\bar{t}_{\text{ins}_m}=\bar{r}_o\frac{(\bar{r}_o+2)}{2\cdot(\bar{r}_o+1)(K\cdot\bar{F}_o)} \tag{17}$$

The first of the graphs in *Figure 4* exhibits the deviation between $\bar{t}_{\text{ins}_m}$ evaluated from (17) and the one evaluated numerically, as a percentage of the theoretical time, for various number of radial increments N. With a coarse mesh of 10 divisions the deviation is $\simeq 4\%$ and drops to $\simeq 1\%$ when the number of radial intervals increases to 90.

In the second test case, also shown in *Figure 4*, the time required for the interface to reach half point between the inner and outer radii was evaluated for a conducting inner radius and properties listed under case A in *Tables 1* and *2*. For this case $\bar{t}_{\varepsilon=0.5(r_o+r_i)}=0.685$ for 10 intervals and 0.735 for 90 radial intervals. Thus it seems that the coarse mesh approached within $\simeq 8\%$ the fine mesh value.

COMPARISON BETWEEN NUMERICAL AND APPROXIMATE ANALYTICAL METHOD

The numerical solutions presented in this work, were compared with results of an approximate analytical method which is especially suitable for low Stefan number problems. The excellent agreement between the results obtained by the two methods when applied to two types of boundary conditions is considered as a proof of the capability for the modified finite differences scheme to handle low Stefan number problems. The two test problems are described below.

Table 1 List of fixed parameters throughout the simulations

$T_f=30°C$	$h_o=3.0\,W/m^2\,°C$
$T_i=20°C$	$F_o=300\,W/m^2$
$T_o=50°C$	$k_s=0.5\,W/m\,°C$
$\rho_l=\rho_s=1000\,Kg/m^3$	$c_{ps}=2.0\,KJ/Kg\,°C$
$r_i=0.01\,m$	$St_{si}=0.1$
$r_o=0.02\,m$	$St_{so}=0.2$
$h_i=0.0\,W/m^2\,°C$ for insulating inner radius	$h_i=10.0\,W/m^2\,°C$ for conducting inner radius
$L=200\,KJ/Kg$	

Initial and boundary conditions:

$G(\bar{r})=-1.0$	$Bi_i=0.2$
$F_i=0.0$	

Table 2 List of varying parameters

	Simulation set			
	A	B	C	D
k_l [W/m °C]	0.75	0.75	0.5	0.5
c_{pl} [KJ/Kg °C]	3.0	2.0	3.0	2.0
$K(=k_l/k_s)$	1.5	1.5	1.0	1.0
St_{li}	0.15	0.1	0.15	0.1
St_{lo}	0.3	0.2	0.3	0.2
F_o	0.4	0.4	0.6	0.6
Bi_o	0.08	0.08	0.12	0.12

Insulated inner radius while the outer surface is exposed to constant heat flux and heat convection with the surrounding

Consider an annulus made of PCM in which initially ($t=0$) the interface coincides with the outer radius and the temperature distribution is uniform and equals the melting temperature. Heat flux from the outer surface will effect the temperature distribution in the outer liquid region and will cause an inward motion of interface. During this process, the initial temperature distribution assures a uniform temperature in the inner solid region. Modifications of (10) to (15) to correspond the particulars of the described situation, yield:

$$St_{li}\frac{\partial\theta_l}{\partial\bar{t}}=\frac{1}{1+\bar{r}}\frac{\partial}{\partial\bar{r}}\left((1+\bar{r})\frac{\partial\theta_l}{\partial\bar{r}}\right) \tag{18}$$

$$\frac{d\bar{\varepsilon}}{d\bar{t}}=-K\frac{\partial\theta_l}{\partial\bar{r}}\bigg|_{\bar{\varepsilon}} \tag{19}$$

$$\theta_l=0 \quad \text{at} \quad \bar{r}=\bar{\varepsilon}(\bar{t}) \qquad \theta_s=0 \quad \text{for} \quad \bar{r}<\bar{\varepsilon}(\bar{t}) \tag{20}$$

$$\bar{\varepsilon}(0)=\bar{r}_o \tag{21}$$

$$\frac{\partial\theta}{\partial\bar{r}}\bigg|_{\bar{r}_o}=Bi_o(\theta_{a_o}-\theta(\bar{r}_o,\bar{t}))+\bar{F} \tag{22}$$

For low Stefan numbers the left hand side of (18) may be neglected such that the right hand side can be integrated to yield:

$$\theta_l(\bar{r},\bar{\varepsilon})=A(\bar{\varepsilon})\ln(1+\bar{r})+B(\bar{\varepsilon}) \tag{23}$$

where A and B are integration constants. Boundary condition at the interface expressed by (18) requires that:

$$B(\bar{\varepsilon})=-A(\bar{\varepsilon})\ln(1+\bar{\varepsilon}) \tag{24}$$

Substituting (24) into (23):

$$\theta_l(\bar{r},\bar{\varepsilon})=A(\bar{\varepsilon})\ln(1+\bar{r}/1+\bar{\varepsilon}) \tag{25}$$

Substituting (25) into (22), the result will be an equation for $A(\bar{\varepsilon})$ which becomes:

$$A(\bar{\varepsilon})=Bi_o\theta a_o+\bar{F}_o\Big/\left(\frac{1}{1+\bar{r}_o}+Bi_o\ln(1+\bar{r}_o/1+\bar{\varepsilon})\right) \tag{26}$$

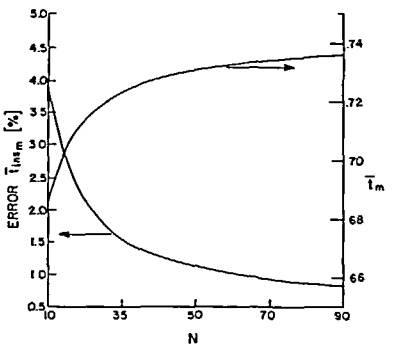

Figure 4 Error in $\bar{t}_{ins_m}$ for simulation case B and melt time $\bar{t}_m$ for simulation case A, as function of the number of radial intervals

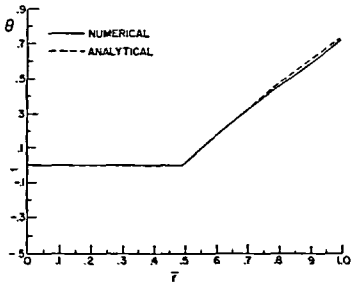

Figure 5 Comparison between numerical and analytical solutions. Temperature distribution when interface is in the midpoint between inner and outer radii. Inner surface insulated outer with convective heat transfer and flux

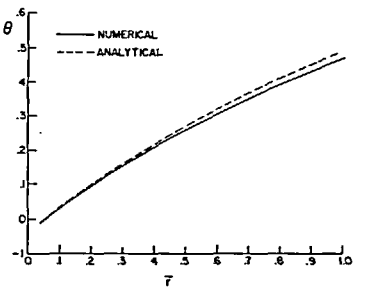

Figure 6 Comparison between numerical and analytical solutions. Temperature distribution when interface is in the 95% point between inner and outer radii. Convective heat transfer on inner and outer surfaces, heat flux on the outer surface

Combining now (26) and (25) and substituting the result in (19):

$$\frac{d\bar{\varepsilon}}{d\bar{t}} = -K\frac{A(\bar{\varepsilon})}{1+\bar{\varepsilon}} \tag{27}$$

which can now be integrated such that:

$$\bar{t} = -\int_{\bar{\varepsilon}}^{\bar{r}_o} \frac{1+\bar{\varepsilon}}{K\cdot A(\bar{\varepsilon})} d\bar{\varepsilon} \tag{28}$$

The left hand side of (28) is known and therefore the integral may be evaluated numerically to provide $\bar{\varepsilon}(\bar{t})$. Radial temperature distribution can be evaluated by substituting $\bar{\varepsilon}(\bar{t})$ in (25).

Figure 5 exhibits the radial temperature distributions at the time when half of the annulus has been melted ($\varepsilon = 0.5(r_i + r_o)$). Results of the analytical and numerical simulation are almost identical. The time required for the interface to reach that point evaluated by the two methods, differs by less than 0.5%.

Heat convection condition on both inner and outer radii while the outer surface is exposed to constant heat flux

This problem starts with the same initial conditions as the previous one. However, heat transfer from the inner radius results in a non-uniform temperature distribution in the solid region. The two region's temperature distributions require a somewhat more complicated solution which is nevertheless quite similar to the previously discussed problem. Following the same steps that led to (25) it can be shown that:

$$\theta_l(\bar{r},\bar{\varepsilon}) = A(\bar{\varepsilon})\ln(1+\bar{r}/1+\bar{\varepsilon}) \qquad 0<\bar{r}<\bar{\varepsilon}(\bar{t}) \tag{29}$$

$$\theta_s(\bar{r},\bar{\varepsilon}) = D(\bar{\varepsilon})\ln(1+\bar{r}/1+\bar{\varepsilon}) \qquad \bar{\varepsilon}(\bar{t})<\bar{r}<\bar{r}_0 \tag{30}$$

with

$$A(\bar{\varepsilon}) = \frac{Bi_o\theta a_o + \bar{F}}{\dfrac{1}{1+\bar{r}_o} + Bi_o\ln(1+\bar{r}_o/1+\bar{\varepsilon})} \tag{31}$$

$$D(\bar{\varepsilon}) = \frac{Bi_i\theta a_i}{\dfrac{1}{1+\bar{r}_i} + Bi_o\ln(1+\bar{r}_i/1+\bar{\varepsilon})} \tag{32}$$

Substituting (31) and (22) into (29) and (30) respectively, the temperature distributions $\theta_s(\bar{r},\bar{\varepsilon})$ and $\theta_l(\bar{r},\bar{\varepsilon})$ in the two regions as function of the interface coordinate $\bar{\varepsilon}$, is determined. The time dependence $\bar{\varepsilon}(\bar{t})$ can now be determined by substituting the obtained θ_s and θ_l into (13) from which:

$$d\bar{t} = \frac{(1+\bar{\varepsilon})d\bar{\varepsilon}}{D(\bar{\varepsilon}) - K\cdot A(\bar{\varepsilon})} \tag{33}$$

Numerical integration of (33) will result in an implicit relation $\bar{\varepsilon}(\bar{t})$ which can be substituted into (29) and (30) to obtain the temperature profiles.

Figure 6 depicts the temperature distributions obtained by the finite differences and analytical methods when the interface has reached 95% of the radial extend of the annulus. Agreement between the two methods although not as good as in the previous case (*Figure 5*), is still excellent. The time required by the interface to reach the 95% point, differ by about 4% between the two methods. The analytical method predicts a faster motion basically because it does not take full account of the sensible heat.

RESULTS AND DISCUSSIONS

The dependence of the melting process and the moving interface which is associated with it, on various parameters of the problem was investigated. For this purpose, four sets of problems were numerically solved. Common to all the sets is a group of parameters which were held constant for all runs. These fixed parameters which are listed in *Table 1*, include all the physical properties of the solid phase as well as the geometry. *Table 2* lists the parameters which are unique to each set. Although dimensionless characteristic groups only effect the solution in each case, typical dimensional parameters are also given to help gain physical orientation. For each set, two different boundary conditions (insulation and heat conduction) were applied on the inner radius. Within a given set, the two boundary conditions are characterized by identical dimensionless groups. Throughout this part of the work (*Figures 7* to *9*), a 60 divisions radial mesh was used. Based on the previously discussed relations between grid size and accuracies, this choice was considered sufficient to demonstrate the results obtained by the modified finite differences scheme.

The purpose of the examples in this study is to concentrate the relative importance of the properties of the liquid phase. In order to obtain an equal base for comparison, all cases start with a solid phase at a uniform temperature such that (15) $G(\bar{r}) = -1.0$, and the initiation of time count $\bar{t}=0$ starts when the outer surface reaches the melting temperature.

The melting time $\bar{t}_m$ for the various simulations is shown in *Table 3*. It seems that the melting time which is of the order of $\bar{t}_m = 1.1$ does not vary appreciably between all the simulated configurations. As expected it is shorter for the insulated inner radius case, but not appreciably so. This fact is due to the relatively small heat exchange areas which are represented by the inner radius. It should also be noted that the melting times in *Table 3* are only slightly smaller than the total insulation melting time. The latter, which is defined as the time required by the flux F_0 to totally melt the PCM when it is initially at the melting temperature T_f is given by (16) and (17). For the geometry and relevant physical properties of the simulation, $t_{ins_m} = 1.39$ h. The difference between this time and those in *Table 3* are due to the fact that in the simulated cases, in addition to the heat flux F_0, there is a convection heat transfer driven by the temperature difference $(T_{a_o} - T_{r_o})$.

Figures 7a and *7b* exhibit the radial temperature distribution at given times for simulation set A. *Figure 7a* is for an insulated inner radius and *Figure 7b* for a conducting one. When the inner radius is insulated, very shortly after the outer radius has reached the melting temperature, the whole cross-section is at an almost uniform temperature close to the melting temperature. When heat is allowed to flow through the inner radius then, throughout the melting process, gradients of temperature are much more noticeable. This almost constant temperature gradient

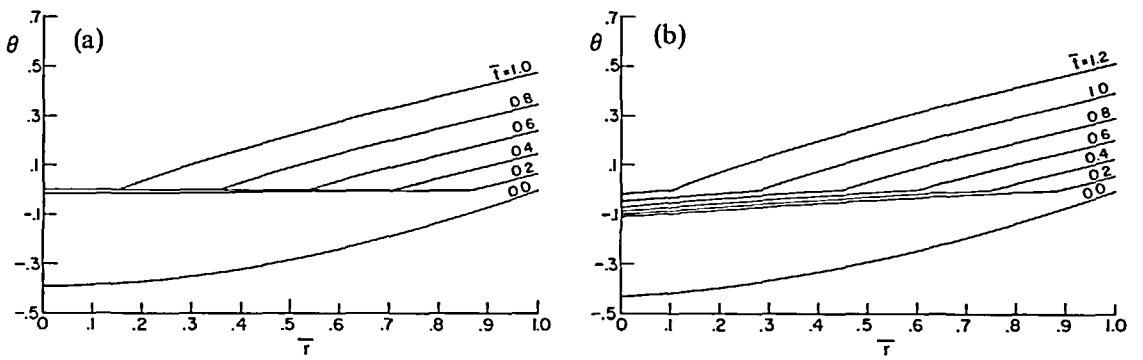

Figure 7 Temperature distribution at various dimensionless time and simulation cases. (a) Insulated inner radius; (b) conducting inner surface

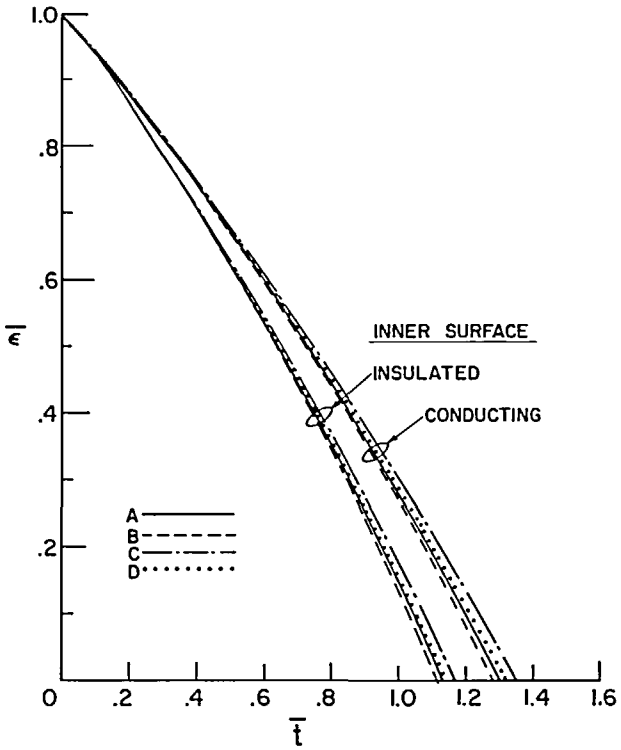

Figure 8 Interface location as function of time for the various simulation cases

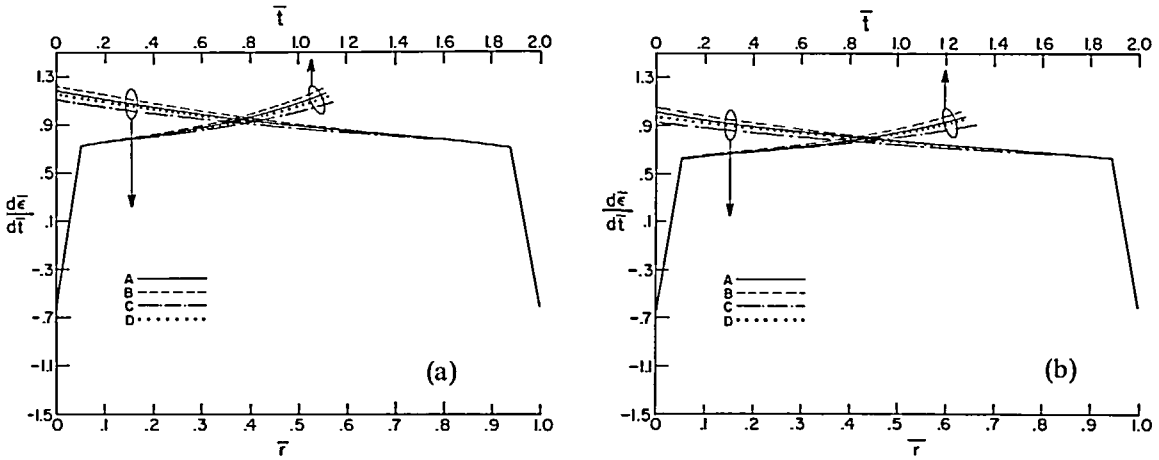

Figure 9 Speed of propagation of the interface as a function of time and radial position for the simulated cases. (a) Insulated inner radius; (b) conducting inner surface

Table 3 Time required to achieve total fusion

	Dimensionless		Dimensional (h)	
Inner radius	Insulated	Conducting	Insulated	Conducting
A	1.11	1.28	1.233	1.422
B	1.11	1.28	1.233	1.422
C	1.15	1.32	1.278	1.467
D	1.12	1.30	1.244	1.444

is the source for energy requirement made by the inner radius. The same sort of behaviour is also exhibited in *Figure 8* where interface location as function of time is depicted. For the insulated inner radius the interface travels faster than for the conducting inner radius case. *Figures 9a* and *9b* depict this interface propagation speed as function of time and radial position for the two inner radius boundary conditions, *Figure 9a* for inner insulated surface and *Figure 9b* for the conducting one. The initial abrupt jump in these Figures, is a result of an attempt to avoid initial singularity so that initially $\zeta = -0.1$ was assumed at the initiation of the melting process.

NOMENCLATURE

Bi Biot number $h \cdot r/k$
C_p specific heat (J/Kg °C)
$F(t)$ heat flux per unit area (W/m^2)
$G(r)$ initial temperature distribution
h heat transfer coefficient (W/m^2 °C)
k thermal conductivity (W/m °C)
K thermal ratio k_l/k_s
L latent heat (J/Kg)
N total number of mesh points in radial coordinates
r radial coordinates (m)
St_{si} Stefan number $Cp_s(T_f - T_i)/L$
St_{li} Stefan number $Cp_l(T_f - T_i)/L$
T temperature (K)
t time (sec)
Δr space step size (m)
α thermal diffusivity $k/C_p\rho$
ε fusion front position in radial direction (m)
ρ density (Kg/m^3)
θ dimensionless temperature
ζ local interface coordinate

Superscript
– dimensionless parameter

Subscripts
a ambient condition
f fusion condition
i inner radial boundary
ins insulated
j running index of radial nodal points
l liquid phase

m melting
o outer radial boundary
q index of radial nodal point nearest the interface
s solid phase

ACKNOWLEDGEMENTS

The authors wish to thankfully acknowledge the help extended by Dr C. Charach of Ben-Gurion University, Israel, in developing the approximate analytical solution as well as his helpful remarks throughout this work.

This research was supported in part by a grant from the Gordon Center for Energy Studies in Tel Aviv University.

REFERENCES

1 Crank, J. Two methods for the numerical solution of moving boundary problems in diffusion and heat flow,' *QJ Mech. Appl. Math*, **10**, 220–231 (1957)
2 Murray, W. D. and Landis, F. Numerical and machine solution of transient heat conduction problems involving melting or freezing, *J. Heat Transf.*, **81**, 106 (1959)
3 Springer, G. S. and Olson, D. R. Method of solution of axisymmetric solidification and melting problems, *ASME Paper, No. 62-WA-246* (1962)
4 Yao, L. S. and Prusa, J. Melting and freezing, in *Advances in Heat Transfer*, (Eds. J. P. Harttnet and T. F. Irvine), Vol. 19, pp 1–95, Academic Press, San Diego (1989)
5 Carslaw, H. S. and Jaeger, J. C. *Conduction of Heat in Solids*, 2nd Edn, Clarendon Press, Oxford (1959)
6 Özisik, M. N. *Heat Conduction*, Wiley, New York (1980)
7 Crank, J., *Free and Moving Boundary Problems*, Clarendon Press, Oxford (1984)
8 Keizman, Y. Numerical solution of a moving boundary problem as a model solution for a solar pipe, *MSc Thesis*, Tel-Aviv Univ. (1989)